Modelling of Reinforced Concrete Core Walls Under Bi-directional Loading

R. Constantin & K. Beyer
Ecole Polytechnique Fédérale de Lausanne (EPFL), Switzerland

15 WCEE
LISBOA 2012

SUMMARY:
Reinforced concrete core walls with open sections are commonly used in practice as a lateral load resisting system for multi-storey buildings. This type of walls has mainly been modelled in the past using simplified models such as plastic hinge models or equivalent frame models. Such models are well suited for addressing the global flexural behaviour of core walls and are commonly used for design purposes. However, shear behaviour or transfer of stresses between the web and the flanges, for example, are either not captured correctly with such models or they are not even addressed. These issues are particularly important when assessing the core wall behaviour under diagonal loading. In order to estimate correctly the above mentioned quantities, a 3D multi-layered shell element model for U-shaped walls is set-up. The local as well as the global behaviour is examined and the behaviour of the wall under diagonal loading is investigated.

Keywords: U-shaped Wall, Shell Model, Diagonal Loading Direction, Out-of-plane Bending

1. INTRODUCTION

Many reinforced concrete (RC) buildings are designed to resist the lateral seismic loads by means of RC core walls. Such walls commonly accommodate staircases or elevator shafts and provide an important part of the lateral load resisting capacity of the building. Common types of RC core walls are the open section core walls, such as U-shaped walls. Their behaviour is complex and relatively unknown as compared to rectangular walls, although they are widely used in practice. Experimental data for such walls is relatively scarce and recent (Reynouard and Fardis, Eds. 2001; Beyer *et al.,* 2008a). Hence rules in design codes were mainly based on experimental results of rectangular walls. However rules for rectangular walls cannot be directly extrapolated to core walls as the behaviour of core walls is considerably more complex than the behaviour of rectangular walls, e.g. with respect to the shear stress distribution between flanges and web. A better understanding of the seismic behaviour of RC core walls is therefore required. A few numerical studies of the inelastic behaviour for U-shaped walls have been performed (Ile and Reynouard, 2005; Mazars *et al.,* 2006; Beyer *et al.,* 2008b; Beyer *et al.,* 2008c) with emphasis on the global response of the wall.

This paper investigates the global as well as the local behaviour of U-shaped walls under complex bi-directional lateral loading. To achieve this, a detailed numerical model is set-up and results are compared to experimental data. The paper gives first a brief overview of the experimental test that is used as reference for the modelling. Next, the set-up of the numerical model is described and the experimental and numerical results are compared in terms of global and local behaviour. Finally, the load transfer of the forces from the wall to the foundation is investigated when the wall is loaded in the diagonal direction.

2. REFERENCE TEST

Two half scale U-shaped walls have been tested under bi-directional quasi-static cyclic loading at ETH Zurich (Beyer *et al.*, 2008a). The two test units differed with regard to their wall thickness: the first test unit (TUA) had a wall thickness of 150 mm while the second one (TUB) had a wall thickness of 100 mm. The reference test used herein is TUA. The cross-section and elevation details for the TUA, the labelling of different wall sections and the displacement loading history applied at the top of the wall are shown in Fig. 2.1 and 2.2, respectively.
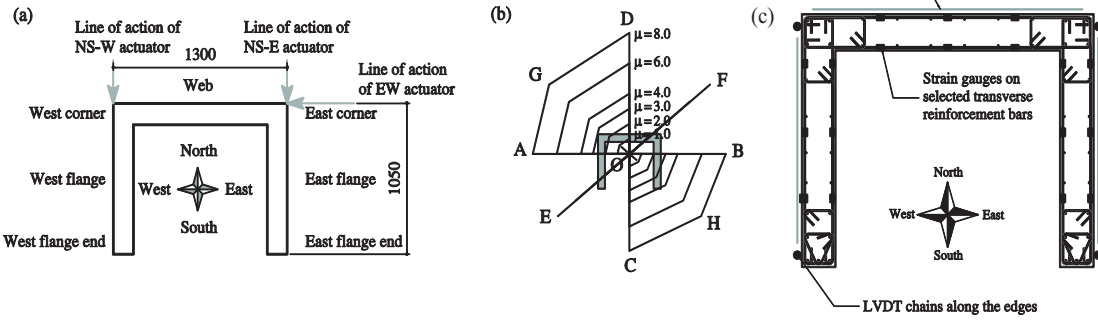

Figure 2.1. (a) Labelling of different wall sections and lines of action of the actuators, (b) bi-directional displacement loading history and (c) wall instrumentation (taken from Beyer *et al.* [2008a]). All dimensions are in *mm*.
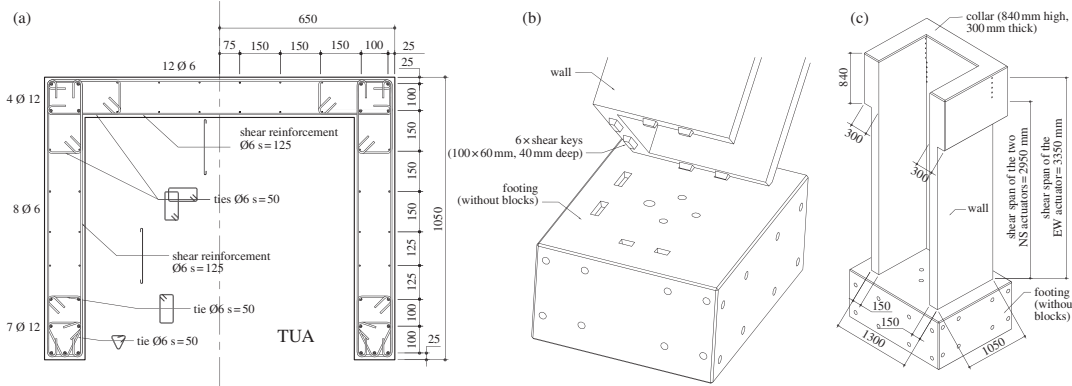

Figure 2.2. TUA geometry: (a) Cross-section, (b) shear keys and (c) elevation (taken from Beyer *et al.* [2008a]). All dimensions are in *mm*.

The test units were subjected to a bi-directional loading history according to the loading pattern shown in Fig. 2.1b:

- reverse cycle parallel to the web (Position A and B, also termed EW cycle) ,
- reverse cycle parallel to the flanges (Position C – flange ends in compression – and Position D – web in compression, also termed the NS cycle),
- reverse cycle (Position E – one flange end in compression – and Position F – one corner in compression, also termed the diagonal cycle)
- "sweep" cycle : O → A→ G→ D→ C→ H→ B→ O

The pattern was repeated at displacement ductility levels of μ_Δ= 1, 2, 3, 4, 6 and 8 until failure. The cycles at μ_Δ= 1 were preceded by four force-controlled cycles at 25%, 50%, 75% and 100% of the predicted first yield lateral force.

During the entire test, the axial force was maintained constant and the rotation of the top of the wall (the wall collar) was restrained by imposing equal displacements at the level of the NS-W and the NS-E actuators (Fig. 2.1a). To investigate the evolution of the rotational stiffness, some small twists were applied at Positions O, A, B, C and D during cycles at ductilities $\mu_\Delta = 1$ and 4; the rotational stiffness is, however, not investigated within the scope of this paper. For further details on the experimental data the reader is referred to Beyer *et al.* [2008a].

3. INELASTIC SHELL MODEL FOR U-SHAPED WALLS

The numerical analyses have been performed using the nonlinear finite element analysis software VecTor4 developed at the University of Toronto (Wong and Vecchio, 2002). This software is dedicated to the analysis of RC plates and shell structures. A smeared rotating crack formulation is employed for the reinforced concrete which is based on the Modified Compression Field Theory (Vecchio & Collins, 1986) and on the Disturbed Stress Field Theory (Vecchio, 2000).

TUA was modelled using multi-layered rectangular shell elements which account for the out-of-plane shear response (Polak and Vecchio, 1993). A number of eight concrete layers of equal thickness were used to model the thickness of the wall. The foundation was not modelled but instead all the degrees of freedom of the nodes at the wall base were restrained. The collar of the wall was modelled with an offset from the mid-surface of the wall so that the loading would be applied at the correct position. The resulting mesh is shown in Fig. 3.1.
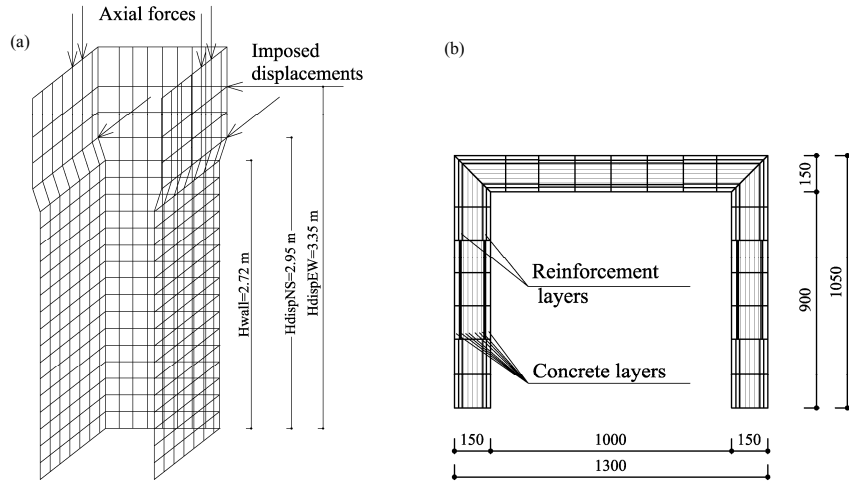

Figure 3.1. Geometry of the shell element model: (a) 3D mid-surface of the mesh and points of load application and (b) cross-section mesh. All dimensions are in *mm* unless otherwise specified in the figure.

The material properties determined from material tests on reinforcement bars and concrete cylinders were used as input parameters for the numerical model. Rupture of the reinforcement bars was, however, not accounted for in the model. The longitudinal and the transversal reinforcements were both modelled as smeared. In addition, for the confined concrete areas of the wall, out-of-plane reinforcement was assigned since the concrete model can account for the tri-axial behaviour of concrete. Perfect bond was assumed between the concrete and the reinforcement. The resulting concrete and reinforcement stress-strain relationships are plotted in Fig. 3.2.

The loading was applied by imposing displacements at the positions of the actuators from the experimental test as shown in Fig. 3.1a and Fig. 2.1a. The NS-E and NS-W displacements were kept equal throughout all loading steps and patterns, restraining the rotation at the top of the wall.
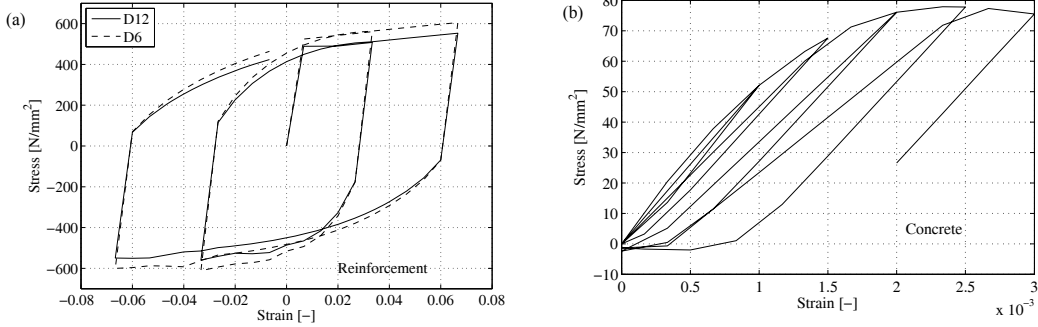
Figure 3.2. Material models: (a) reinforcement model and (b) concrete model: unconfined concrete in cyclic compression.

4. COMPARISON OF NUMERICAL AND EXPERIMENTAL RESULTS

4.1. Global behaviour: force-displacement hysteresis

The global behaviour of the wall is studied in terms of force-displacement hysteresis plotted individually for each loading direction: the EW direction (Positions A and B), the NS direction (Positions C and D) and the diagonal direction (Positions E and F). Results from pushover and cyclic analyses are compared to the experimental results (Fig. 4.1). Separate cyclic analyses were performed along these three directions; a full displacement load history was not performed so far because of large computational expense and convergence problems.
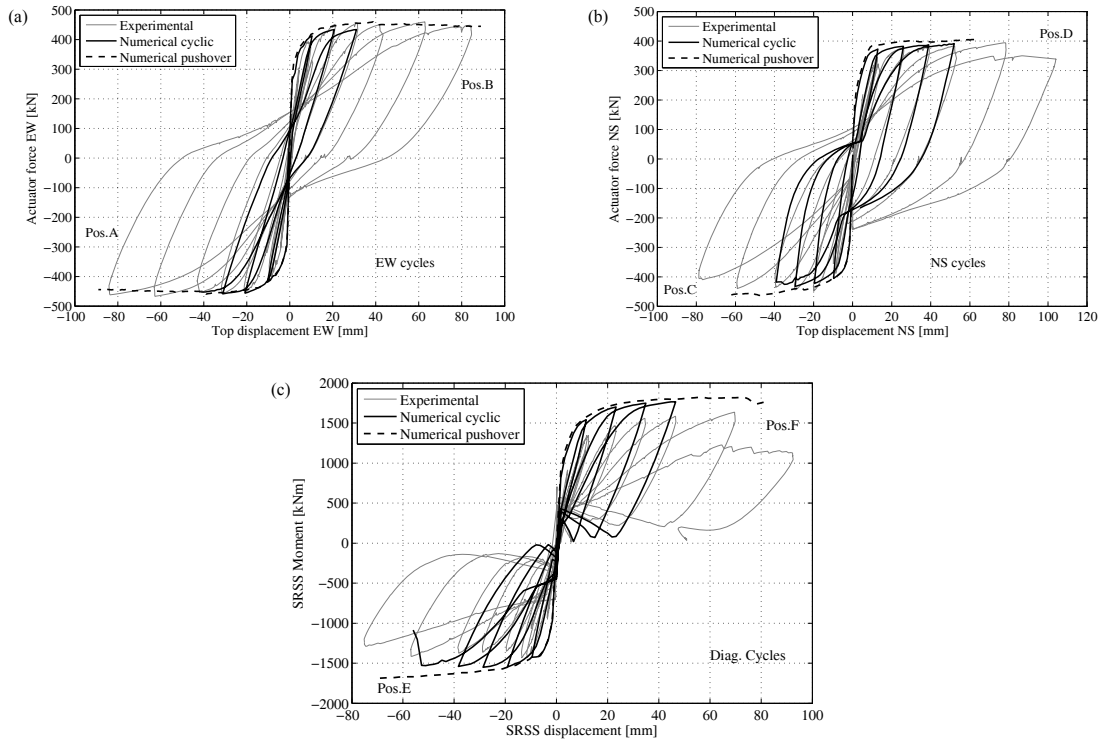

Figure 4.1. Comparison of the results obtained from VecTor4 with the experimental results: Force-displacement hystereses for cycles in the EW and the NS directions (a-b). Moment-displacement hystereses for the diagonal direction (c). Pushover analyses results are also included (a-c).

There is a good match of the numerical results with the experimental ones in terms of force capacity and hysteresis shape for the loading directions EW (parallel to the web) and NS (parallel to the flanges). For the diagonal direction, the pushover analysis as well as the cyclic analysis overestimates by approximately 25% the experimental values of the moment capacity. It was, however, argued (Beyer *et al.,* 2008b) that the moment capacities reached during the experiments for the diagonal direction were not the ultimate moment capacities of the wall for that direction. Within the cycles of one ductility level, the wall was loaded in diagonal direction after it had been loaded in the two principal directions (EW and NS direction). Hence, when the wall was loaded in the diagonal direction, the stiffness was reduced and as a result the full moment capacity was not reached at Positions E and F. To investigate whether the shell element model is able to capture the behaviour in the diagonal direction, it is therefore necessary to perform an analysis with the full displacement loading history.

4.2. Local behaviour

The local behaviour of the wall was investigated in terms of the vertical strain profile at Position E and in terms of curvature profiles at Positions A, B, C, D, E and F at ductility μ_Δ= 3.0.
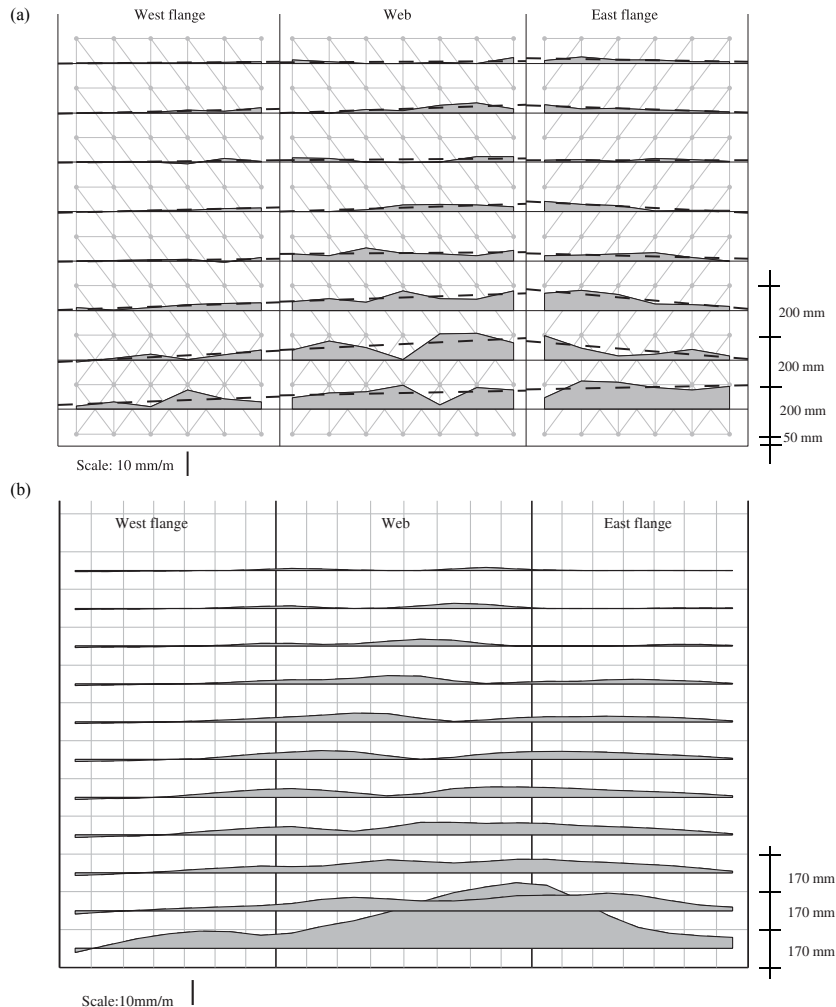

Figure 4.2. Comparison of the results obtained from VecTor4 with the experimental results at Position E during the μ_Δ= 3.0 cycles (at Position E the west flange end is in compression): (a) vertical strain profile of the wall experimentally determined from Demec measurements and (b) vertical strain profile of the wall numerically determined.

4.2.1. Vertical strain profile
The vertical strain profile computed from Demec measurements (Fig. 4.2a) is compared to the numerically determined vertical strain profile (Fig. 4.2b). The Demec measurements were taken on the inside faces of the wall, recording the vertical strain values over equal vertical distances of 200 mm and starting 50 mm above the base as it is shown in Fig. 4.2a. The numerical vertical strain values were computed as average vertical strains of the elements in the model mesh shown in Fig. 3.1a. All elements in the mesh had a height of 170 mm, as shown in Fig. 4.2b and the average vertical strains were computed from the vertical displacements of the four corner nodes of each rectangular element.

Considering the vertical strain values shown in Fig. 4.2 and the heights over which they have been computed the numerical values match in general and the experimental values of the vertical strains rather well. The vertical strains computed from the numerical model tend to concentrate stronger towards the base while the experimental ones are more distributed over the height of the wall. Note, however, that the experimental strains computed from the base crack opening are not included in Fig. 4.2a. At the end of the west flange, it can be, however, noticed that the experimental strains indicate vertical tensile strains for the flange end which is compression, whereas the numerical strains are compressive strains. This can be explained by looking at the deformed shape of the wall at Position E at the peak of the μ_Δ= 3.0 cycle (Fig. 5.3). Near the base of the wall (Fig. 5.3d) the west flange presents horizontal out-of-plane bending, with the inside part of the flange end in tension while the outside part is in compression. The Demec measurements were taken on the inside face of the wall, hence the tensile vertical strains. The numerical strain values are computed from the vertical displacements of the nodes in the mid-surface of the wall, which explains the compressive strains. The overall vertical strain profile from numerical results is found therefore to be consistent with the experimental one.

4.2.2. Curvature profile
The experimentally determined curvatures, from LVDT measurements, are plotted against the numerically determined curvatures in Fig. 4.3. Experimental values of the curvatures were determined from the LVDT chains along the four outside edges of the wall (Fig. 2.1c). The numerical values of the curvatures were determined from the vertical displacements of the nodes in the mesh at the same four edges of the wall where the LVDT chains were positioned.

Numerically determined curvatures for the EW direction (Position A and B) fit the experimental curvature values with some discrepancies: the predicted curvature profile indicates the presence of important shear cracks in the web, which were not noticed during the experiments. For Positions D and F the results match fairly well, while for Positions C and E the predicted curvatures underestimate the experimental values of the curvatures at heights of about 0.2 of the wall height.

5. BEHAVIOUR UNDER DIAGONAL LOADING

Beyer *et al.* (2008a) argued that the diagonal loading direction is the most complex one in terms of load transfer mechanism. Therefore in order to gain a better understanding of the behaviour of the wall under diagonal loading, the transfer of forces from the wall to the foundation, as well as the deformed shape of the wall, was investigated. The following section presents these results obtained with the numerical model described in Section 3, with emphasis on Position E, when the west flange end is in compression.

5.1. Transfer of forces from wall to foundation

The distribution of reaction forces at the base of the wall, in Position E at a displacement ductility of μ_Δ= 3, is presented in Fig. 5.1. As expected, the shear forces are transferred from wall to foundation mainly within the compressed zones. The distribution of the vertical reaction forces indicates that the compressed zones develop at the end of the west flange, as expected, but also at the corner of the west flange and the web. The assumption of "plane sections remaining plane" is therefore no longer valid.
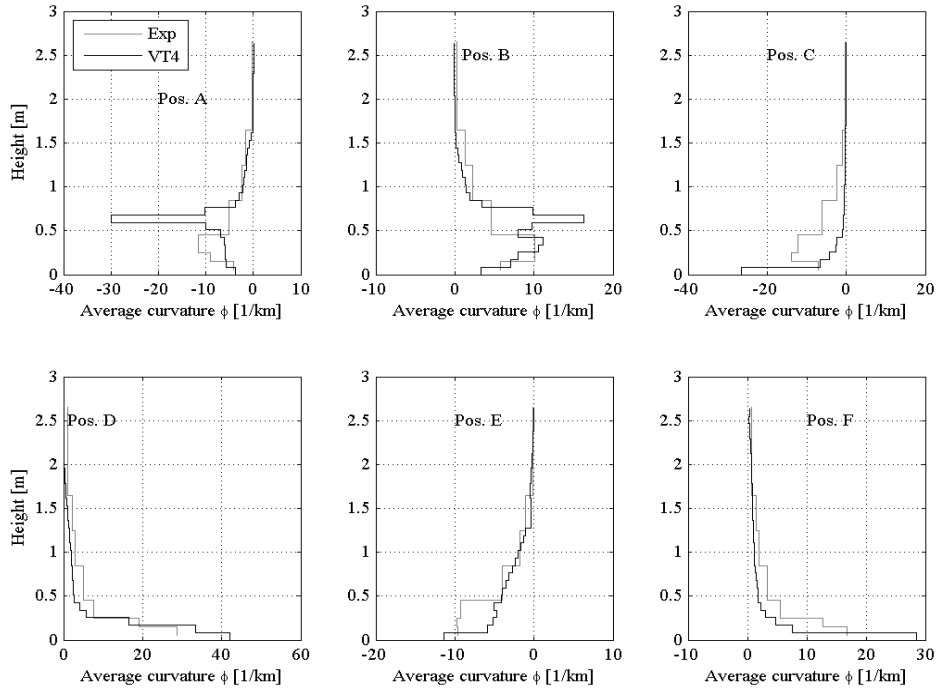
Figure 4.3. Comparison of the results obtained from VecTor4 with the experimental results during the $\mu_\Delta = 3.0$ cycles at Positions A, B, C, D, E and F: curvatures numerically determined from the nodal displacements of the mesh elements (VT4) compared with curvatures experimentally determined from LVDT measurements.

Table 5.1 summarises the distribution, between different wall sections, of the total applied shear force in the X and in the Y direction, transferred from the wall to the foundation. For the X direction, the reactions at the corner nodes between the flanges and the web are counted towards the web, while for Y direction, the same corner nodes are counted towards the flanges.
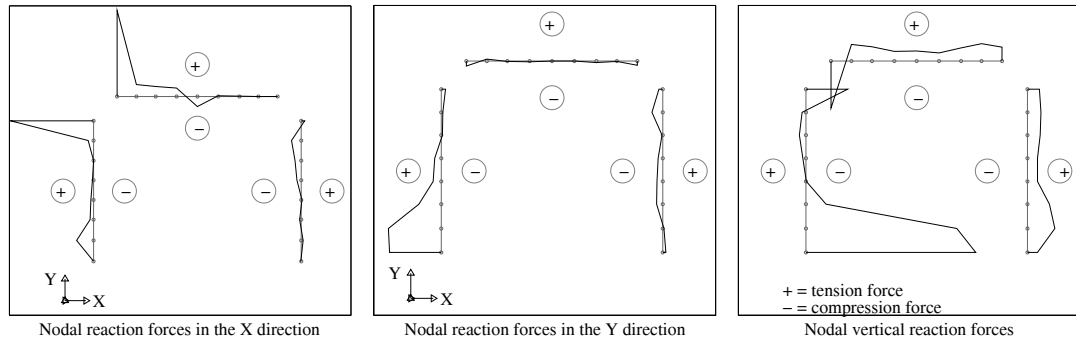

Nodal reaction forces in the X direction | Nodal reaction forces in the Y direction | Nodal vertical reaction forces

Figure 5.1. Numerically determined qualitative distribution of reaction forces at the base of the wall at Position E at the peak of the $\mu_\Delta = 3$ cycle (at Position E the west flange end is in compression).

Table 5.1. Numerically determined distribution of reaction forces at the base between the web and flanges at Position E at the peak of the $\mu_\Delta = 3$ cycle (at Position E the west flange end is in compression).

Reaction component (Position E)	West flange	Web	East flange
Shear force in the X direction	15%	83%	2%
Shear force in the Y direction	124%	~0%	-24%

As expected, the shear force in the X direction is mainly transferred through the web (83% of the applied shear force in the X direction). The west flange takes approximately 15% of the shear force in the X direction as an out-of-plane shear force, mainly through the compressed zones next to the corner and at the free end of the west flange.

The west flange transfers to the foundation approximately 124% of the total shear force applied in Y direction while the reaction forces in the east flange are of the opposite sign and account for 24% of the applied shear force. The large shear force in the Y direction that is transferred by the west flange to the foundation is the result of two effects: 1) the east flange is under tension and therefore has limited in-plane shear carrying capacity and 2) since the rotation at the top of the wall is restrained, a torsional moment in the wall appears, which produces additional in-plane shear forces in the wall sections.
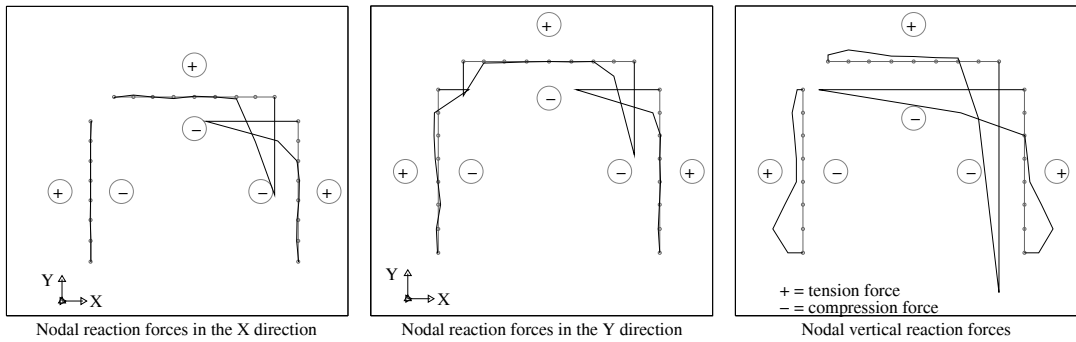
Nodal reaction forces in the X direction	Nodal reaction forces in the Y direction	Nodal vertical reaction forces

+ = tension force
− = compression force

Figure 5.2. Numerically determined qualitative distribution of reaction forces at the base of the wall at Position F at the peak of the μ_Δ= 3 cycle (at Position F the corner of the web and of the east flange is in compression).

Table 5.2. Numerically determined distribution of reaction forces at the base between the web and flanges at Position F at the peak of the μ_Δ= 3 cycle (at Position F the corner of the web and of the east flange is in compression).

Reaction component (Position F)	West flange	Web	East flange
Shear force in the X direction	-1%	94%	7%
Shear force in the Y direction	16%	21%	63%

For Position F, when the corner between the web and the east flange is in compression, the distribution of reaction forces is shown in Fig. 5.2 with the amount of shear force transferred by each wall section to the foundation summarised in Table 5.2. The distribution of reaction forces indicates that the compressed zone is now limited only to the compressed corner, where most of the shear forces are transferred from the wall to the foundation. In this case the assumption of the "plane sections remaining plane" still holds approximately. As indicated in Table 5.2, almost the entire shear force in the X direction is transferred through the web, as expected. It is interesting to notice that approximately 20% of the shear force in the Y direction is transferred to the foundation through the web as an out-of-plane force. As in the case of loading to Position E, the out-of-plane shear force is transferred through the part of the wall which is under compression, namely the east corner of the web.

5.2. Deformed shape of the wall

The deformed shape of the wall at Position E at a displacement ductility of μ_Δ= 3 is shown in Fig. 5.3. The mid-surface of the mesh elements (undeformed and deformed) is plotted three-dimensionally and at representative cross-sections of the wall over its height: at fractions of 0.06, 0.2 and 1 of the wall height, termed as cross-section 0.06 (CS0.06), cross-section 0.2 (CS0.2) and cross-section 1 (CS1), respectively. It can be seen that the web as well as the west flange deform in out-of-plane bending close to the base of the wall (Fig. 5.3c, d, e).

Again at the base of the west flange, the nodes of the mesh deform in an arched shape (Fig. 5.3b) suggesting an arch action between the two compressed zones at the corner and the end of the west flange. At the top of the wall the rotation is restricted (Fig. 5.3f).
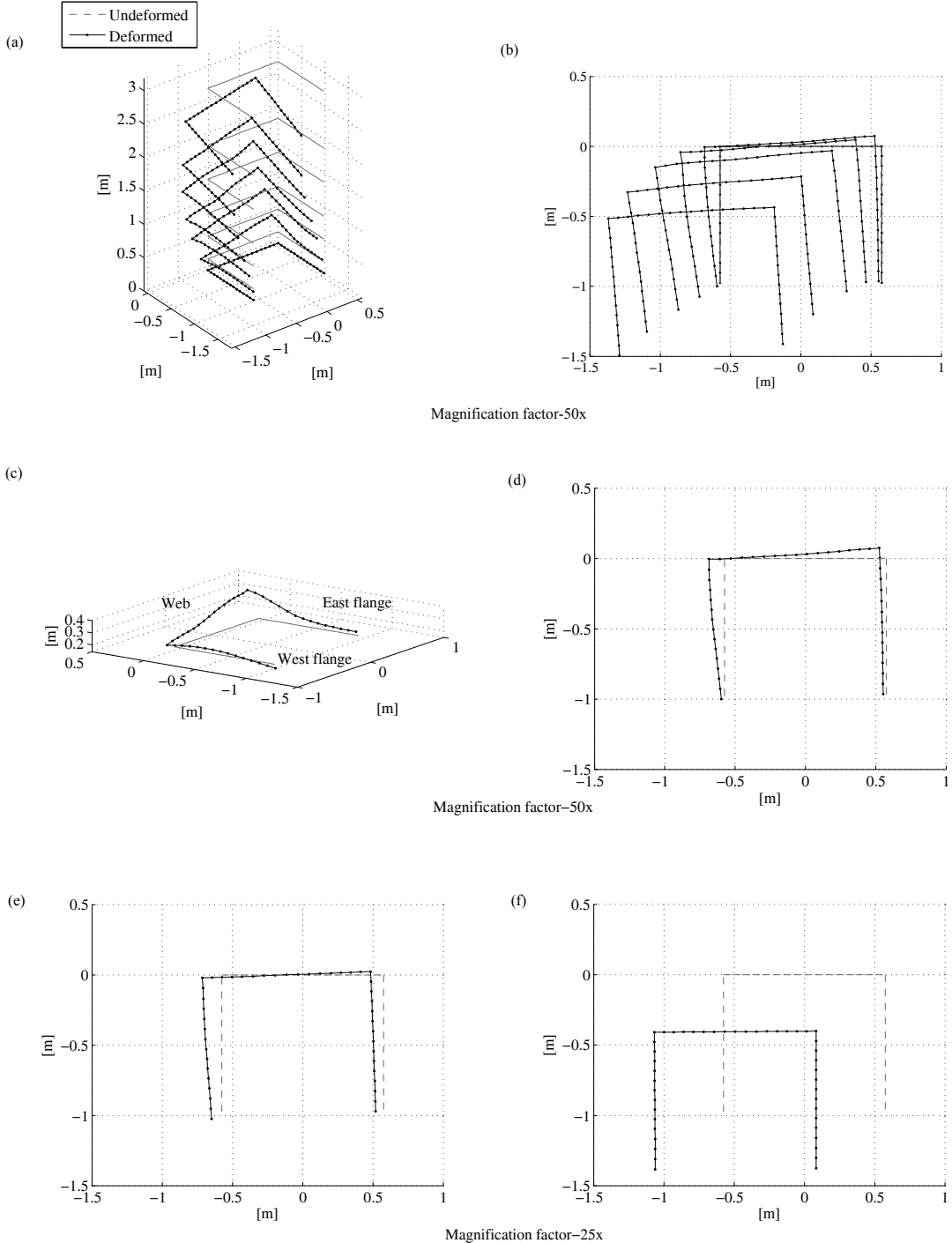

Figure 5.3. Numerically determined deformed shape of the wall at Position E at the peak of the $\mu_\Delta = 3$ cycle (at Position E the west flange end is in compression): (a) 3D deformed shape, (b) 3D deformed shape – view from the top, (c) 3D deformed shape of the element nodes for CS0.06, (d) CS0.06, (e) CS0.2 and (f) CS1. The displacements were magnified by factors of 50 or 25 as indicated below the subfigures.

6. CONCLUSIONS AND OUTLOOK

The objective of this article was to investigate the diagonal behaviour of RC U-shaped walls under bi-directional lateral loading. For this purpose a shell element model was set-up and used for investigating the load transfer of forces from the wall to the foundation under diagonal loading.

Predicted global force capacities from separate cyclic analyses along each direction matched fairly well with the experimental results, except for the diagonal loading direction where the predicted moment capacity was higher than in the experiments. A full displacement loading history needs to be applied to check whether the model can accurately predict the experimental values of the moment for the diagonal loading direction, this being the next step in validation of the shell element model.

Local behaviour in terms of vertical strains was checked for the diagonal direction, at Position E, and found to be predicted in a satisfactory manner. The curvatures were checked for several loading directions and some discrepancies were found at Positions A and B (EW cycles). Shear and flexural deformations should be compared separately to find the source of these differences.

It was also found that under diagonal loading, approximately 15% to 20% of the shear force is transferred to the foundation as an out-of-plane force either by the flanges (when the flange end is in compression), or the web (when the corner of the web and of the flange is in compression). Furthermore, at diagonal loading with one flange end in compression, the assumption of "plane sections remaining plane" was found to be no longer valid. Compression zones appeared at the end of the flange and also at its corner with the web. These zones were responsible for the transfer of the shear forces from the wall to the foundation. A complex deformed shape with out-of-plane bending in the web and in the west flange suggest that further efforts need to be directed in understanding the load path of forces through the wall from the load application points to the foundation for the diagonal loading direction.

REFERENCES

Beyer, K., Dazio, A. and Priestley, M.J.N. (2008a). Quasi-static tests of two U-shaped reinforced concrete walls. *Journal of Earthquake Engineering* **12:7**, 1023-1053.

Beyer, K., Dazio, A. and Priestley, M.J.N. (2008b). Inelastic wide-column models for U-shaped reinforced concrete walls. *Journal of Earthquake Engineering* **12:S1**, 1-33.

Beyer, K., Dazio, A. and Priestley, M.J.N. (2008c). Elastic and inelastic wide-column models for RC non-rectangular walls. *Proceedings of the 14th World Conference on Earthquake Engineering*, Beijing, China.

Ile, N. and Reynouard, J.M. (2005). Behaviour of U-shaped walls subjected to uniaxial loading and biaxial cyclic lateral laoding. *Journal of Earthquake Engineering* **9:1**, 67-94.

Mazars, J., Kotronis, P., Raguneau, F. and Casaux, G. (2006). Using multifiber beams to account for shear and torsion applications to concrete structural elements. *Computer Methods in Applied Mehcanics and Engineering* **195**, 7264-7281.

Polak, M.A. and Vecchio, F.J. (1993). Nonlinear analysis of reinforced concrete shells. Journal of structural Engineering **119:12,** 3439-3462.

Reynouard, J.M. and Fardis, M.N., Editors (2001). Shear wall structures. Thematic report No. 5, Lisbon, Portugal.

Vecchio, F.J. and Collins, M.P. (1986). The modified compression-field theory for reinforced concrete elements subjected to shear . *ACI Journal* **83:2**, 219-231.

Vecchio, F.J., Lai, D., Whim, W. and Ng, J. (2001). Disturbed stress field model for reinforced concrete: Validation. *Journal of Structural Engineering* **127:4**, 350-358.

Wong, P. and Vecchio, F.J. (2002). VecTor2 and Formworks Manual. University of Toronto, Department of Civil Engineering, Canada.